Brucella abortus MFP: A Trimeric Coiled-Coil Protein with Membrane Fusogenic Activity[†]

Mariela del Carmen Carrica,*[,‡] Patricio Oliver Craig,[§] Silvia del Valle Alonso,[||] Fernando Alberto Goldbaum,[§] and Silvio Lorenzo Cravero[‡]

Instituto de Biotecnología, CICVyA, INTA, Los reseros y las cabañas s/n, Castelar, Buenos Aires, Agentina, Fundación Instituto Leloir (IIBBA-CONICET), Av Patricias Argentinas 435, Buenos Aires, Argentina, and Laboratorio de Biomembranas, Universidad Nacional de Quilmes, R. Saenz Peña 352, Bernal, Buenos Aires, Argentina

Received March 18, 2008; Revised Manuscript Received May 24, 2008

ABSTRACT: The bacterial genus *Brucella* consists of a group of facultative intracellular pathogens which produces abortion and infertility in animals and a chronic debilitating febrile illness in humans. BMFP is a basic protein of *Brucella abortus* that belongs to a highly conserved group of homologue proteins of unknown structure and function in proteobacteria (COG2960). In this study, we report the structural and biochemical characterization of this protein. We found that BMFP has two structural domains: a carboxyl-terminal coiled-coil domain through which the protein self-associates as a trimer and a natively disordered amino-terminal domain which has propensity to adopt an amphipathic α-helical structure. This natively unfolded domain undergoes a structural rearrangement from unfolded to α-helix in the presence of high ionic strength, acidic pH, detergents, and phospholipid vesicles. Moreover, we demonstrated that the interaction of BMFP with phospholipid vesicles promotes in vitro membrane fusion. These results contribute to the elucidation of the structural and functional properties of this protein and its homologues present in most proteobacteria.

Brucella spp. is a facultative intracellular Gram-negative bacterium that belongs to the α-2-proteobacteria group. They are pathogenic for many mammalian species, including humans, causing an illness called Brucellosis. This is a chronic infection that produces abortion and sterility in domestic mammals and a chronic undulant fever in humans (*1*).

In comparison with other pathogenic bacteria, *Brucella* spp. lacks classical virulence factors such as exotoxins, invasive proteases, toxic lipopolysaccharide, capsules, virulence plasmids, and lysogenic phages. Furthermore, it does not generate resistance forms, does not display antigenic variation, and lacks fimbriae, pili, and flagella (*2*).

Brucella spp. virulence resides mostly in its ability to survive and multiply within professional and nonprofessional phagocytes (*3, 4*). To do this, *Brucella* perturbs the maturation of the phagosome, subverts vesicular trafficking within infected eukaryotic cells, and creates a unique intracellular niche in which it multiplies (*5, 6*). Moreover, it has been shown that the early acidification of phagosomes to a pH of 4.0−4.5 following the *Brucella* infection is crucial for intracellular survival (*7*).

Mutagenesis studies have identified a number of factors, including smooth lipopolysaccharide, stress response proteins, response regulators, metabolic genes, and a secretion system, required for virulence in vitro and in animal models (*8–11*).

In this report, we characterized the product of ORF BAB1_1543 of *Brucella melitensis* biovar *abortus* 2308, which was denominated BMFP protein. It is totally conserved in all *Brucella* species that have been sequenced up to date, and it is also conserved in a wide variety of proteobacteria. In spite of this, no BMFP-like protein has been characterized; therefore, it has no readily identifiable homologues in the repository of experimentally determined high-resolution structures in the Protein Data Bank (*12*), and its function is unknown.

In vitro characterization of native purified proteins has proven to be a useful strategy for investigating protein function. With the aim of analyzing the structure and shedding light on a probable biological activity of BMFP, we performed a biophysical and biochemical characterization of this protein. These experiments allowed us to obtain a model of BMFP structure and demonstrate that this protein interacts with phospholipids and promotes vesicle fusion in vitro. These results contribute to the elucidation of the structural and functional properties of this protein and related homologues.

EXPERIMENTAL PROCEDURES

Bacterial Strains and Growth Conditions. Escherichia coli strains were grown in Luria-Bertani medium. The BTH101

[†] This work was supported by grants from INTA (Proyecto Nacional 472-AESA 2581), the Howard Hughes Medical Institute international, and the Agencia Nacional de Promoción Científica y Tecnológica, Argentina.

* To whom correspondence should be addressed. Telephone: (54 11) 4621-1447. Fax: (54 11) 4621-1447. E-mail: carricamariela@yahoo.com.ar.

[‡] CICVyA, INTA.

[§] Fundación Instituto Leloir (IIBBA-CONICET).

[||] Universidad Nacional de Quilmes.

10.1021/bi800462y CCC: $40.75
Published on Web 07/11/2008

strain was grown at 30 °C, whereas DH5α and BL21 strains were grown at 37 °C, unless otherwise noted. Appropriate antibiotics were added to the following final concentrations: 100 μg/mL ampicillin, 25 μg/mL kanamycin, and 10 μg/mL chloramphenicol. In the BTH[1] assay, 5-bromo-4-chloro-3-indolyl-β-D-galactopyranoside (X-gal) was added to a final concentration of 40 μg/mL in agar plates containing both Amp and Km. Colonies from each pairwise combination were restreaked, inoculated into 20 mL of LB, and grown for 16 h at 28 °C for subsequent quantification of β-galactosidase activity in a standard Miller assay.

DNA Manipulations. Plasmids pET24D-BMFP (encoding BMFP), pET24D-BMFP-N (encoding BMFP amino acids 1−48), pET24D-BMFP-C (encoding BMFP amino acids 50−101), pET24D-BMFPL12W (encoding BMFP with the L12W mutation), pET24D-BMFPS106W (encoding BMFP with the S106W mutation), pET24D-BMFPT (encoding BMFP with thrombin cleavable sites between the histidine tag and the protein), and pET24D-BMFPCT (encoding BMFP amino acids 50−101 with thrombin cleavable sites between the histidine tag and the protein) were generated by polymerase chain reaction (PCR) from *Brucella abortus* S2308 chromosome DNA using suitable primers, and cloning of the products between the *Nco*I and *Xho*I sites of the pET24D vector (Novagen) in frame with the T7 promoter. All the products included a six-histidine tag fused to the C-terminal end of the proteins.

PCR from *B. abortus* S2308 chromosome DNA using suitable primers was also used to amplify the coding sequence of the full-length BMFP and truncated variants BMFP-N (amino acids 1−48) and BMFP-C (amino acids 50−101) and perform their cloning between the *Xba*I and *Kpn*I restriction sites of BTH vectors (pUT18C and pKT25) in frame with *Bordetella pertussis* adenylate cyclase fragments (*13*).

Expression and Purification of Recombinant Proteins. pET24D plasmids encoding the sequences of BMFP, BMFP mutants, or BMFP truncated variants were transformed in *E. coli* BL21(DE3). The cells were grown in LB at 37 °C to an A_{600} of 0.5 and induced with 1 mM isopropyl β-D-thiogalactoside (IPTG) for 4 h. Cells were harvested by centrifugation at 3000*g* for 20 min, resuspended in binding buffer (Qiagen), and disrupted by sonication with a probe tip sonicator. The total cell lysates were centrifuged at 14000*g* for 30 min to remove nonsoluble protein, cell debris, and unbroken cells. Binding and elution from nickel nitrilotriacetic acid−agarose resin were carried out under native conditions according to the manufacturer's instructions (Qiagen). Eluted proteins were dialyzed against 1× PBS. Proteins were assayed with a Coomassie blue-based staining solution.

To obtain proteins without the histidine tag (used for vesicle interaction, fusion, and aggregation assays), the proteins containing thrombin cleavable site were cleaved with thrombin (10 units/mg of protein) by incubation at 16 °C overnight.

Vesicle Preparation. Phospholipids were purchased from Avanti Polar Lipids (Birmingham, AL) and from Sigma. L-α-Dipalmitoylphosphatidylcholine (DPPC) and L-α-dipalmitoylphosphatidic acid (DPPA) were cosolubilized in chloroform in different molar ratios, dried under N_2, resuspended in buffer [50 mM Tris-HCl (pH 8.0)], and sonicated to yield small unilamellar vesicles (SUV) or extruded through two stacked polycarbonate filters (Nucleopore, 0.1 μm pore size) to yield large unilamellar vesicles (LUV).

Limited Proteolysis. Purified full-length BMFP was incubated at 28 °C with 1 μg/mL trypsin (Sigma). Protease treatments were stopped at different time points by addition of 1% TFA. All the digestion products were examined via Tris-Tricine SDS−PAGE. To identify the protected fragments, N-terminal sequencing by Edman degradation was performed on electroblotted PVDF membranes and the C-terminus was mapped on the basis of the molecular weight of the cleavage products analyzed by mass spectrometry.

Chemical Cross-Linking. Purified BMFP, BMFP-N, and BMFP-C were cross-linked with ethylene glycol bis(succinimidylsuccinate) (EGS) (Sigma) used at concentrations of 0.5, 1.0, and 5.0 mM. The reactions were carried out for 30 min at room temperature in 1× PBS buffer and stopped by addition of 50 mM Tris-HCl (pH 8.0). Cross-linked products were analyzed via Tris-Tricine SDS−PAGE.

Determination of the Molecular Weight by Static Light Scattering. The average molecular weights (M_w) of BMFP, BMFP-N, and BMFP-C were determined on a Precision Detector PD2010 light scattering instrument tandemly connected to a high-performance liquid chromatography system and an LKB 2142 differential refractometer. The samples were loaded on a Superdex 75 or Superdex 200 column and eluted with PBS buffer. The 90° light scattering and refractive index signals of the eluting material were recorded on a personal computer and analyzed with Discovery32, supplied by Precision Detector. The 90° light scattering detector was calibrated using bovine serum albumin (66.5 kDa) as a standard.

Circular Dichroism Spectroscopy. The circular dichroism (CD) spectra of BMFP, BMFP-N, and BMFP-C in the far-UV region (250−200 nm) were measured on a Jasco J-810 spectrophotometer under different experimental conditions using quartz cuvettes with a path length of 0.1 cm. Samples were incubated for at least 30 min before CD measurements were taken. The CD spectra were analyzed with K2D (http://www.embl-heidelberg.de/~andrade/k2d/) (*14*) to evaluate the secondary structure content.

Thermal denaturation was followed by measuring the protein molar ellipticity at 222 nm by slowly increasing the temperature with a Peltier system (Jasco). The range of temperature scanning was 25−90 °C at a rate of 2 °C/min.

Tryptophan Fluorescence Spectroscopy. Tryptophan intrinsic fluorescence measurements were taken on a Molecular Devices SpectroMAX GeminiEM spectrofluorimeter using

[1] Abbreviations: COG, cluster of orthologous groups; X-gal, 5-bromo-4-chloro-3-indolyl-β-D-galactopyranoside; BTH, bacterial two-hybrid; PCR, polymerase chain reaction; IPTG, isopropyl β-D-thiogalactoside; LB, Luria-Bertani medium; PBS, phosphate-buffered saline; DPPC, L-α-dipalmitoylphosphatidylcholine; DPPA, L-α-dipalmitoylphosphatidic acid; SUV, small unilamellar vesicles; LUV, large unilamellar vesicles; TFA, trifluoroacetic acid; SDS−PAGE, sodium dodecyl sulfate−polyacrylamide gel electrophoresis; PVDF, polyvinylidene fluoride; EGS, ethylene glycol bis(succinimidylsuccinate); CD, circular dichroism; DLS, dynamic light scattering; NBD-PE, *N*-(7-nitro-2,1,3-benzoxadiazol-4-yl)phosphatidylethanolamine; Rh-PE, *N*-(lissamine rhodamine B sulfonyl)phosphoethanolamine; DPA, sodium dipicolinate; EDTA, ethylenediaminetetraacetic acid; T_m, melting temperature; RI, refractive index.

an opaque 96-well plate. The protein concentration was 10 μM. Samples were excited at 295 nm, and the fluorescence emission was measured in the 300−400 nm wavelength range.

Determination of the Vesicle Diameter by Dynamic Light Scattering. Measurements of vesicle diameter by DLS were carried out with a Malvern ZetaSizer Nano-S apparatus. Small unilamellar vesicles were made in 50 mM Tris-HCl buffer (pH 8.0) and were filtered with a 0.2 nm pore size filter before measurements. The SUV concentration used was 250 μM, and the protein concentration was 1 μM.

Turbidity Assay. Turbidity measurements were taken on a Multiskan Spectrum double-beam spectrophotometer (Thermo Electro Corp.) by using 1 cm matched silica cuvettes at 400 nm. The SUV concentration was 250 μM. The lipid:protein ratio for the turbidity assays was kept at 50:1.

Liposome Fusion Assays. The time course of liposome fusion after addition of 1 μM protein was measured by a group of different assays. In all experiments, the vesicle concentration was 100 μM.

Lipid Mixing Assay. Membrane fusion was analyzed by lipid mixing between unlabeled LUV and LUV labeled with *N*-(7-nitro-2,1,3-benzoxadiazol-4-yl)phosphatidylethanolamine (NBD-PE) and *N*-(lissamine rhodamine B sulfonyl)-phosphoethanolamine (Rh-PE) in a 4:1 molar ratio. This assay is based on the resonance energy transfer between NBD (donor) and Rho (acceptor). An efficient energy transfer is observed when both fluorescent lipids are in the same LUV at a 0.6:0.6:100 molar ratio. When the labeled vesicles are fused with unlabeled ones, a lipid mixing that dilutes the fluorescent lipids and decreases the efficiency of the energy transfer is produced. The percentage of lipid mixing is calculated by comparison with a control sample in which a 100% lipid mixture is produced by addition of 0.2% (v/v) Triton X-100.

Lipid mixing was followed in time via the increase in donor fluorescence (NBD-PE) with the excitation and emission monocromators set at 465 and 530 nm, respectively.

The extent of lipid mixing was determined according to the following equation:

$$\%\text{lipid mixing} = [(F_t - F_0)/(F_{max} - F_0)] \times 100$$

where F_0 is the value of the initial fluorescence of LUV labeled with both probes and unlabeled LUV, F_t is the value of fluorescence after incubation for t minutes with the protein, and F_{max} is the value of fluorescence after addition of Triton X-100 to maximally disperse the probes (*15*).

Internal Content Mixing. Liposomes were prepared containing either 5 mM terbium chloride, 50 mM sodium citrate, 10 mM Tris/HCl (pH 7.4), or 50 mM sodium dipicolinate (DPA) and 10 mM Tris-HCl (pH 7.4). In both cases, nonencapsulated material was removed by gel filtration of the liposomes using Sephadex G-25 (Pharmacia) equilibrated with iso-osmolar 50 mM NaCl, 1 mM EDTA, and 10 mM Tris-HCl (pH 7.4). Zero percent and 100% fluorescence (aqueous content mixing) were taken as the intrinsic fluorescence intensity of the Tb/DPA-labeled liposome mixture and the fluorescence obtained after vesicle lysis with 0.2% *n*-dodecyl maltoside in assay buffer without EDTA as described by Duzgunes et al. (*16*). Fluorescence measurements were carried out at 25 °C using a Molecular Devices SpectroMAX GeminiEM spectrofluorometer.

RESULTS

BMFP Is Conserved across Diverse Bacterial Species. BMFP is a 106-residue basic protein [UniProtKB entry Q2YLY4 (Figure 1A)] that has a large number of homologues in proteobacteria. These proteins correspond to the COG2960 cluster of orthologous groups that has 204 members (pFAM February 2008) (http://pfam.sanger.ac.uk/) (*17*). A sequence alignment of a subset of these orthologous proteins from diverse species is shown in Figure 1B. The average percentage of sequence identity of all proteobacterial proteins of COG2960 is 37%.

Analysis of the BMFP sequence using PredictProtein (http://www.predictprotein.org/) (*18*) indicates a high helical content (68%) corresponding to two helices encompassing residues R7−N43 and R50−E85 which span the N-terminal and C-terminal halves of the protein, respectively (Figure 1A). Besides, Paircoil (http://groups.csail.mit.edu/cb/paircoil/cgi-bin/paircoil) (*19*) predicted two coiled-coil regions: a high-score region comprising residues R50−G86 that span the C-terminal helix and a low-score region comprising residues N6−S36 that span the N-terminal helix (Figure 1A,C). In this regard, it is worth noting that although the C-terminal coiled-coil prediction was conserved in all the representative members of COG2960, few exhibited a coiled coil predicted in the amino-terminal half, which could argue against the existence of this feature in the BMFP structure. A helical wheel representation shows that the predicted N-terminal helix is highly amphipathic, whereas the predicted C-terminal helix, although amphipathic, has a more uniform distribution of polar and nonpolar residues (Figure 1A).

On the basis of these analyses, we designed two truncated forms of BMFP comprising residues 1−48 (named BMFP-N) and 50−101 (named BMFP-C) with the aim of conducting a comparative analysis and dissecting the contribution of each region to the structure of the full-length protein.

BMFP Self-Associates as a Trimer through a Coiled-Coil Domain Located in the C-Terminal Half of the Protein. Coiled-coil structures are involved in protein−protein homomeric and heteromeric interactions. To test if BMFP self-associates in vivo, we used a bacterial two-hybrid (BTH) system. In this BTH assay, test proteins are fused to two adenylate cyclase fragments (AC18 and AC25) and cotransformed in an *E. coli* adenylate cyclase-deficient strain (BTH101) (*13*). The isolated cyclase fragments are inactive, but their activity is restored when they are brought together through the association of the fused proteins. These interactions and recovering of adenylate cyclase activity are detected through the activation of specific promoters that switch on the transcription of the LacZ gene.

The β-galactosidase activity was increased up to the level of the positive control when the BTH101 strain was cotransformed with both AC18 and AC25 fused either to the full-length BMFP or BMFP-C. By contrast, no β-galactosidase activity was detected when both of the cyclase subunits were fused to BMFP-N or when one of the fragments was fused to BMFP-N and the other to BMFP-C (Figure 2A). These results indicate that BMFP self-associates in vivo by the carboxyl-terminal half of the protein.

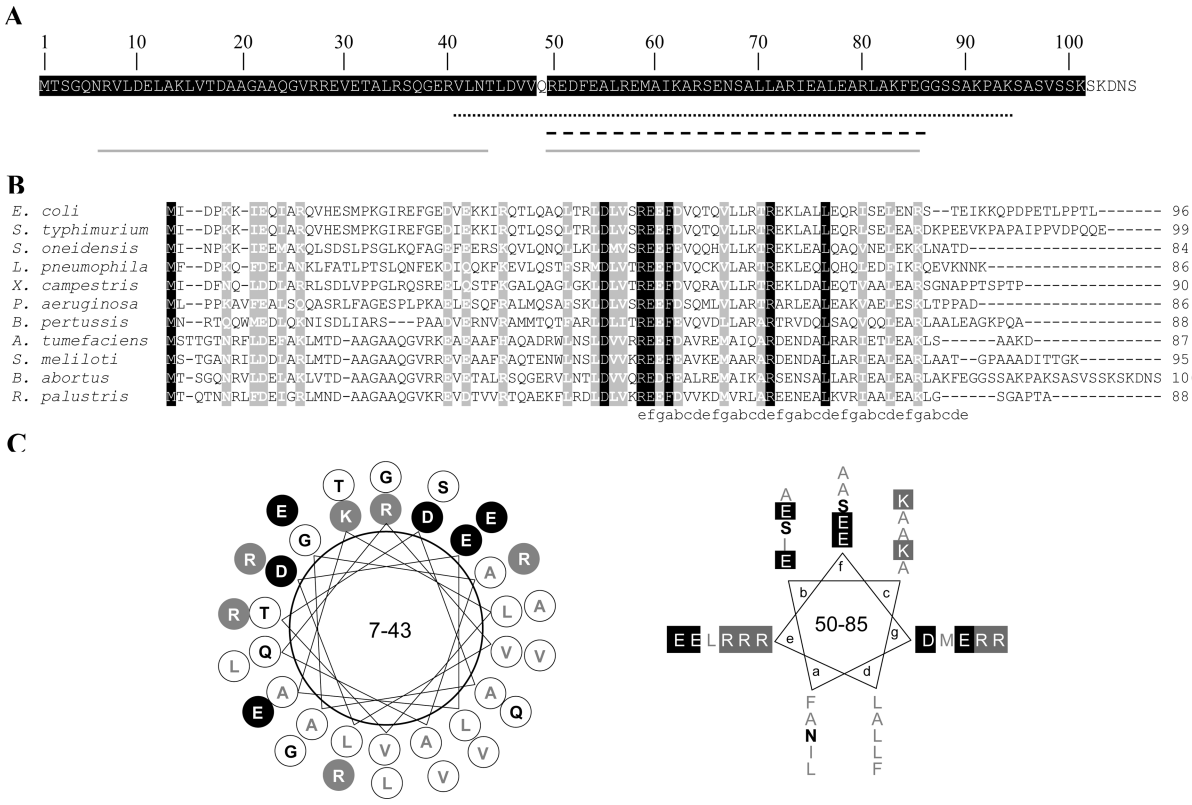

FIGURE 1: Sequence analysis of BMFP. (A) BMFP scheme. The predicted helical (solid gray line) and coiled-coil regions (black dashed line) and the protease resistant core (dotted black line) are indicated. The sequences corresponding to the truncated forms of BMFP (BMFP-N and BMFP-C) are indicated in white letters on a black background. (B) ClustalW alignment of 11 representative protein homologues of COG2960 (*E. coli*, *Salmonella typhimurium*, *Shewanella oneidensis*, *Legionella pneumophila*, *Xanthomonas campestris*, *Pseudomonas aeruginosa*, *Bo. pertussis*, *Agrobacterium tumefaciens*, *Sinorhizobium meliloti*, *B. abortus*, and *Rhodopseudomonas palustris*). Identical residues are shown in white on a black background, whereas similar residues are shown in white on a gray background. The positions of the heptad repeats were assigned using Paircoil and are indicated at the bottom of the alignment. (C) Helical wheel scheme of the predicted N-terminal (residues 7−43) and C-terminal (residues 50−85) helices. The periodicity used for the N-terminal helix was 18/5, corresponding to an undistorted α-helix, whereas for the C-terminal helix it was 7/2, due the possible implication of this helix in a coiled-coil structure. Residues are represented in gray letters for nonpolar residues, black bold letters for polar uncharged residues, white letters on a black background for negatively charged residues, and white letters on a gray background for positively charged residues.

To investigate the stoichiometry of the complex, we performed chemical cross-linking and static light scattering experiments. Chemical cross-linking of isolated BMFP and BMFP-C shielded trimers as the largest products when the amount of cross-linking reagent was increased. By contrast, no cross-linking of BMFP-N was observed under the same conditions (Figure 2B). Moreover, analysis of BMFP, BMFP-C, and BMFP-N by static light scattering coupled to size exclusion chromatography showed single homogeneous peaks with molecular masses of 40.6, 21.0, and 6.8 kDa, respectively, in agreement with a trimeric structure of BMFP (M_w for monomer = 13.4 kDa) and BMFP-C (M_w for monomer = 6.9 kDa), and a monomeric structure of BMFP-N (M_w for monomer = 6.4 kDa) (Figure 2C). No dimeric or monomeric species were observed for BMFP or BMFP-C. The light scattering experiments were repeated several times at different protein concentrations (1−5 mg/mL), and we observed the same results. These experiments indicate that under the conditions that were assayed only trimers of BMFP and BMFP-C and monomers of BMFP-N are significantly populated and demonstrate that BMFP self-associates as a trimer through its carboxyl-terminal coiled-coil region.

The Amino-Terminal Half of BMFP Is Disordered. Conformational parameters such as solvent accessibility, flexibility, and local unfolding propensity are responsible for the protease cleavage susceptibility of specific sites along the polypeptide chain (*20*). We performed a limited proteolysis analysis of BMFP to characterize the conformational state and dissect the structural domains of this protein. The enzyme used was trypsin, which cleaves the polypeptide chain at the carboxyl terminus of basic residues. These residues are uniformly distributed in BMFP. At short time exposures, we observed that the carboxyl-terminal half of the protein remained intact, whereas the N-terminal half was more susceptible to cleavage. With longer exposures (more than 1 h), the C-terminal tail was also cleaved and a protease-resistant core could be observed between V41 and K94 (Figure 3). This protease-resistant core contained the predicted C-terminal coiled-coil domain. In this regard, it has to be noted that although K91 is not predicted to be part of the coiled coil, the presence of proline at the carboxylic side of this residue would prevent its tryptic cleavage (*21*). Similarly, the presence of E51 at the carboxylic side of R50 would reduce the extent of the tryptic cleavage of this residue.

Circular dichroism (CD) spectroscopy was used to analyze the secondary structure of BMFP and its carboxyl- and amino-terminal domains. The CD spectrum of BMFP and BMFP-C, measured in 50 mM Tris-HCl, 150 mM NaCl buffer (pH 8.0), exhibited double minima at 208 and 222 nm, indicating the prevalence of helical structure (Figure 4A).

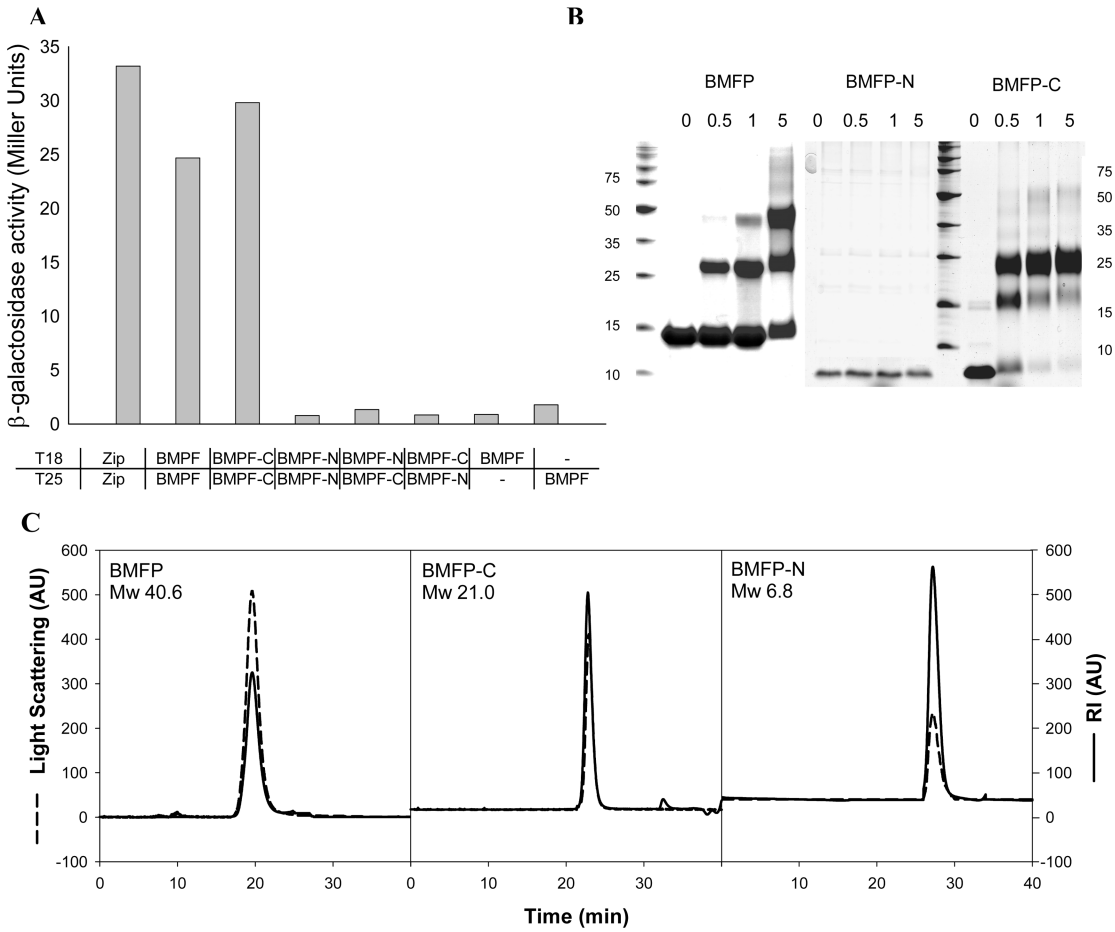

FIGURE 2: Quaternary structure analysis of BMFP. (A) Bacterial two-hybrid analysis of BMFP, BMFP-C, and BMFP-N self-interaction and the heteromeric interaction of BMFP-C and BMFP-N. Full-length BMFP and truncated BMFP were fused with T18 or T25 adenylate cyclase fragments and cotransformed in *E. coli* strain BTH101. Bacteria were grown in LB at 30 °C and were analyzed for *β*-galactosidase activity. A representative experiment is shown. (B) Chemical cross-linking of BMFP, BMFP-N, and BMFP-C. Cross-linked products were separated via 15% SDS−PAGE followed by Coomassie brilliant blue staining. Protein markers are shown in kilodaltons. The numbers 0, 0.5, 1, and 5 indicate the millimolar concentrations of ethylene glycol bis(succinimidyl succinate) that were used. (C) Gel filtration coupled to SLS analysis of BMFP, BMFP-N, and BMFP-C. The proteins were run on a Superdex-75 column and eluted with 50 mM Tris-HCl, 150 mM NaCl buffer (pH 8). The molecular mass of each protein was calculated relating its light scattering at 90° (dashed line) and RI (solid line) signals, and comparison of this value with that obtained for BSA as a standard.

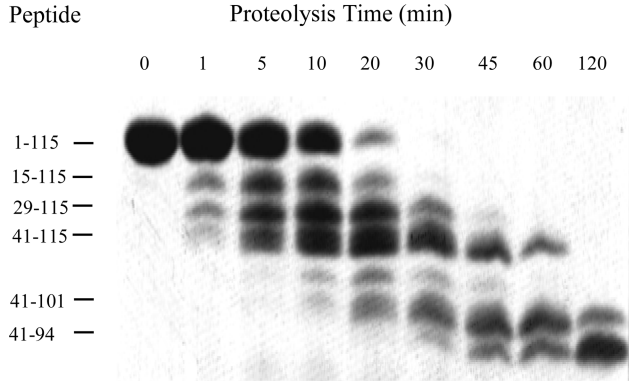

FIGURE 3: Limited proteolysis of BMFP. Shown is the Tricine SDS−PAGE separation of the peptides produced by the digestion of BMFP with trypsin as a function of time. At the top is shown the proteolysis time and at the left the sequence range encompassing the peptides. In this experiment, we used BMFP fused to a His tag in the carboxyl-terminal end of the protein so the total length is 115 residues.

The percentage of helical structure of these proteins, estimated through the analysis of their CD spectra using K2D (http://www.embl-heidelberg.de/~andrade/k2d/) (*14*) (Table 1), agrees with the percentage of amino acids involved in the predicted carboxyl-terminal coiled coil of BMFP and BMFP-C (34 and 70%, respectively). On the other hand, the magnitude of the CD signal of BMFP-N was very low, indicating that the N-terminal domain is disordered. These results agree with the fact that this was the first region to be cleaved by proteases in the limited proteolysis experiments. The spectrum of BMFP-N was practically identical to that theoretically calculated by the difference between the full-length BMFP and BMFP-C spectra, indicating that under the conditions that were tested there is no significant stabilization of the N-terminal domain through any contact with the C-terminal half of the protein or between contiguous N-terminal domains in the trimeric structure of the protein.

Thermal unfolding experiments with BMFP, BMFP-N, and BMFP-C were performed by monitoring the ellipticity at 222 nm as a function of temperature. The melting temperatures of BMFP and BMFP-C were 58.2 and 59.6 °C, respectively, and the observed conformational transitions were fully reversible. BMFP-N exhibited no conformational change because under the condition that we tested this domain was already unfolded (Figure 4B).

The Disordered Domain Undergoes a Structural Rearrangement under Different Conditions. Disordered regions

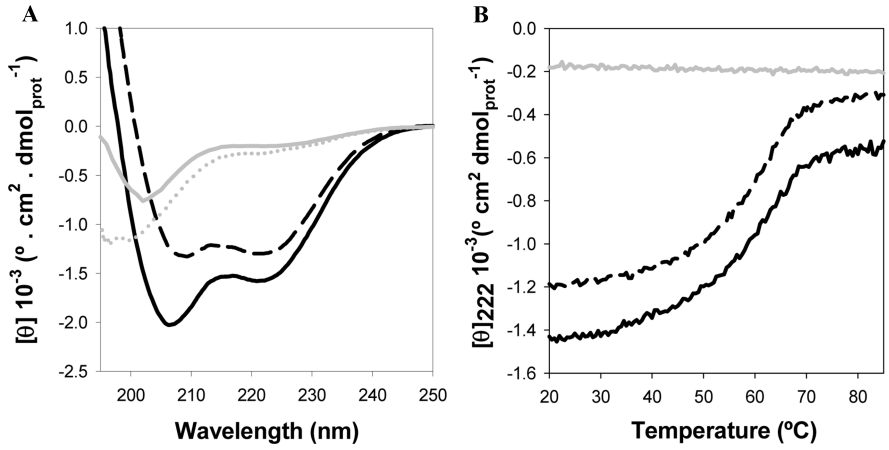

FIGURE 4: CD analysis of BMFP and truncated variants. Far UV-CD spectra (A) and heat-induced denaturation curves (B) of BMFP (black solid line), BMFP-C (black dashed line), and BMFP-N (gray solid line). The spectrum of BMFP-N calculated by subtraction of the BMFP and BMFP-C spectra is also indicated (gray dotted line). Thermal denaturation was analyzed by measurement of the molar ellipticity at 222 nm as a function of temperature. All measurements were taken in 50 mM Tris-HCl, 150 mM NaCl buffer (pH 8.0).

Table 1: Secondary Structure Analysis of BMFP and Truncated Variants, Estimated by the Analysis of their CD Spectra Using K2D

	% α-helix	% β-sheet	% random coil
BMFP	30	16	54
BMFP-N	8	45	47
BMFP-C	70	3	26

Table 2: Secondary Structure Increment of BMFP and Truncated Variants under Different Conditions

	BMFP[a]	BMFP-N[a]	BMFP-C[a]
0.4 M sodium phosphate (pH 8.0)	40.3	171.7	3
0.4 M sodium sulfate (pH 8.0)	31.8	6.6	7.6
1.2 M sodium chloride (pH 8.0)	26.4	0.8	5.4
50 mM sodium acetate (pH 4.0)	31.3	20	0
5 mM SDS (pH 8.0)	19.3	310.8	0
DPPC SUV (pH 8.0)[b]	47.5	225.4	6.1
75:25 DPPC/DPPA SUV (pH 8.0)[b]	74.1	381.4	5.3

[a] The values indicate the percentage of increment in the molar ellipticity at 222 nm of each protein in comparison to their signal in 50 mM Tris-HCl (pH 8.0). [b] The lipid:protein molar ratio that was used was 60 for BMFP and BMFP-C and 250 for BMFP-N.

in proteins have been shown to be involved in a variety of functions and frequently undergo disorder-to-order transitions upon binding to their natural ligands or environmental changes (*22, 23*). According to the previously published results, we decided to test probable conformational changes of BMFP, BMFP-N, and BMFP-C under different conditions (ionic strength, polyvalent anions, detergent, pH, etc.). Table 2 shows the increase in the molar ellipticity at 222 nm under each condition in comparison to the proteins in 50 mM Tris-HCl (pH 8.0).

The effect of the ionic strength at pH 8.0 was tested using sodium salts of three different anions: phosphate, sulfate, and chloride. All these ions produced an increase in the α-helix content of BMFP, and at the same ionic strength, the effect was maximal for phosphate (Figure 1A and 2A of the Supporting Information). Phosphate also produced an important increment in the CD signal of BMFP-N and a significant increment in the thermal transition midpoint of BMFP and BMFP-C (69.7 and 75.3 °C, respectively). However, no change in the BMFP-C CD signal was observed under the same conditions. On the other hand, significant changes in the secondary structure of BMFP and BMFP-N were observed in the presence of sodium dodecyl sulfate (SDS) at pH 8.0, whereas no change was produced in the BMFP-C structure (Figure 1B of the Supporting Information). The T_m under this condition could not be measured due to the noncooperativity of the transition. Finnally, a decrease in the pH to pH 4.0 produced an increment in the CD signal of the full-length BMFP, but no significant change in BMFP-C or BMFP-N.

All these results are indicative that the N-terminal region of BMFP undergoes a disorder to order transition in the presence of phosphate and SDS and that phosphate also stabilizes the carboxyl-terminal half of the protein. Surprisingly, acidic pH, sulfate, and chloride ions produce an increase in the secondary structure content of BMFP but not of BMFP-N. These results suggest that these compounds have a low capacity to induce structure in the monomeric N-terminal domain, but in the trimeric state, they are effective because of the probable existence of contacts between neighbor domains that help to further stabilize the induced structure.

BMFP Interacts with Phospholipid Vesicles and Undergoes a Structural Rearrangement. The increase in the level of structure of BMFP produced by the addition of phosphate and SDS, and the occurrence of trimeric coiled coils in several membrane fusion proteins (*24, 25*), prompted us to investigate the interaction of this protein with phospholipids. Therefore, we measured the CD spectrum of BMFP in the presence of the lipid surface provided by small unilamellar vesicles (SUV) composed of different ratios of L-α-dipalmitoylphosphatidic acid (DPPA) and the zwitterionic L-α-dipalmitoylphosphatidylcoline (DPPC). Under all conditions, we observed a significant increase in the level of structure of BMFP by the addition of SUV. The maximal effect was produced by 75:25 DPPC/DPPA SUV (Table 2 and Figure 5). The structure induced was circumscribed to the N-terminal half of the protein, while no change was observed in BMFP-C at the same SUV composition.

The lipid:protein ratio that produced the maximum increase in the magnitude of the CD signal at 222 nm was 60 for BMFP and 260 for BMFP-N (Figure 3 of the Supporting Information). This difference probably arises as a consequence of an avidity effect that enhances the strength of the binding of the trimeric N-terminal domain of BMFP to vesicles as compared to monomeric BMFP-N.

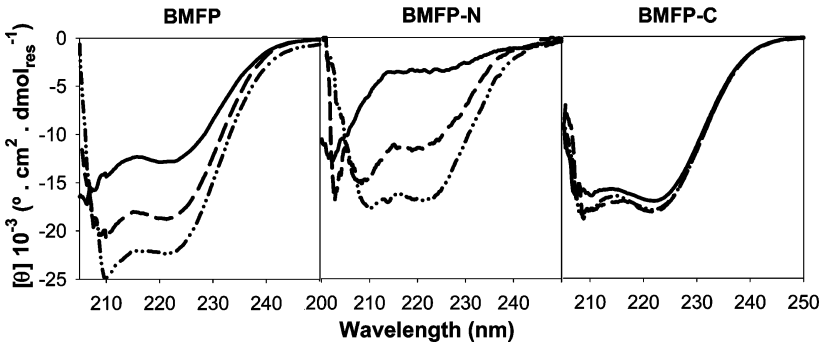

FIGURE 5: Effect of small unilamellar vesicles on the secondary structure of BMFP and truncated variants. Far-UV CD spectra were recorded in 50 mM Tris-HCl buffer (pH 8.0) in the presence of SUV composed of DPPC (dashed line) or DPPC and DPPA 75:25 (dashed−dotted line). The lipid:protein molar ratio was 60 for BMFP and BMFP-C and 260 for BMFP-N. The spectrum of each protein in 50 mM Tris-HCl buffer (pH 8.0) (solid line) is also shown as a reference.

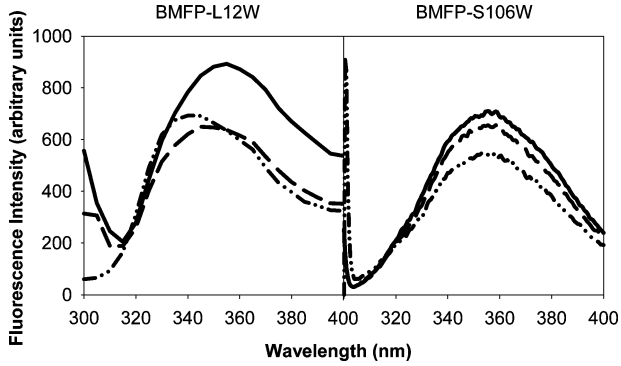

FIGURE 6: Intrinsic fluorescence emission of BMFP-L12W and BMFP-S106W mutants in the presence or absence of phospholipid vesicles. Spectra were recorded in 50 mM Tris-HCl (pH 8.0) in the presence of neutral vesicles composed of DPPC (dashed line) or negatively charged vesicles composed of DPPC and DPPA (75:25) (dashed−dotted line). The lipid:protein molar ratio was 50. The spectrum of each mutant in 50 mM Tris-HCl buffer (pH 8.0) (solid line) is shown as a reference. The excitation wavelength was 295 nm.

These results suggest that a rearrangement in BMFP structure is produced, where the N-terminal domain undergoes a transition from random coil to an amphipatic α-helix that is stabilized by interaction with lipid vesicles. To test this hypothesis, we decided to take advantage of the environmental polarity sensitivity of tryptophan intrinsic fluorescence. Due to the fact that wild-type BMFP contains no Trp residues in its sequence, we designed two Trp single mutants (BMFP-L12W and BMFP-S106W) to probe the polarity changes in the environment of different regions of BMFP produced upon interaction with vesicles. In the BMFP-L12W mutant, the Trp residue was located at the hydrophobic side of the hypothetical amphipathic α-helix of the N-terminal domain, whereas in the BMFP-S106W mutant, the mutated Trp was located at the end of the C-terminal coiled-coil domain. The secondary structure conservation of both single mutants proteins with respect to wild-type BMFP was confirmed by circular dichroism (Figure 4 of the Supporting Information).

In 50 mM Tris-HCl buffer (pH 8.0), we observed a maximum emission wavelength (λ_{max}) of 355 nm for both BMFP-L12W and BMFP-S106W, indicating a complete exposure to the solvent of these residues (Figure 6). The BMFP-S106W λ_{max} remains invariable in the presence of SUV. By contrast, BMFP-L12W exhibited a significant blue shift of its fluorescence emission (λ_{max} = 338−340 nm) in the presence of DPPC/DPPA SUV, in agreement with the interaction of the amphipathic α-helix with the hydrophobic core of the lipid vesicles. At the same lipid concentration and lipid:protein ratio (50:1), SUV composed solely of DPPC produced a more slight shift to the blue (λ_{max} = 345 nm) for BMFP-L12W. However, the shift was increased and reached a λ_{max} of 340 nm with an increase in lipid concentration (Figure 5 of the Supporting Information). This result indicated that the vesicle−protein interaction is more efficient with negatively charged vesicles than with neutral vesicles.

BMFP Induces Liposome Aggregation and Fusion in Vitro. To establish whether purified BMFP and its domains (BMFP-C and BMFP-N) could induce membrane aggregation and fusion, we assessed their behavior with phospholipid vesicles in several in vitro assays used to study viral and intracellular membrane fusion (*15, 16, 26*).

To analyze the liposome aggregation, we measured the increase in turbidity and average size of vesicles produced after addition of protein. Turbidity was evaluated by absorbance measurement at 400 nm, and vesicle size was analyzed by dynamic light scattering using SUV composed of a mixture of DPPC and DPPA in a 75:25 molar ratio at neutral pH. An increase in the turbidity and average size of SUV was observed with addition of BMFP, while BMFP-C and BMFP-N produced no increase in the turbidity of the solution, although a slight increase in the average size of the vesicles was observed (Figure 7A and Table 3).

Due to the fact that the increase in the magnitude of the scattering signal and vesicle size could be caused both by vesicle aggregation or fusion, we specifically evaluated the protein fusogenic potential through two different fluorometric assays that detect "lipid mixing" and "aqueous content mixing". Lipid mixing was evaluated by FRET using liposomes (LUV) labeled with NBD-PE and Rho-PE, whereas aqueous content mixing was evaluated by measuring the fluorescence of the Tb−DPA complex produced upon fusion of liposomes containing $TbCl_3$ or DPA encapsulated in their aqueous interior phase. BMFP produced a significant lipid and aqueous content mixing (Figure 7B). Also, BMFP-N produced lipid and aqueous content mixing, although the efficiency was significantly lower than that of the full-length protein. By contrast, BMFP-C produced no significant fusion as evidenced by both assays. In this regard, it has been noted that the slight increase in vesicle size induced by BMFP-C described before could probably arise as a consequence of some vesicle aggregation produced by this

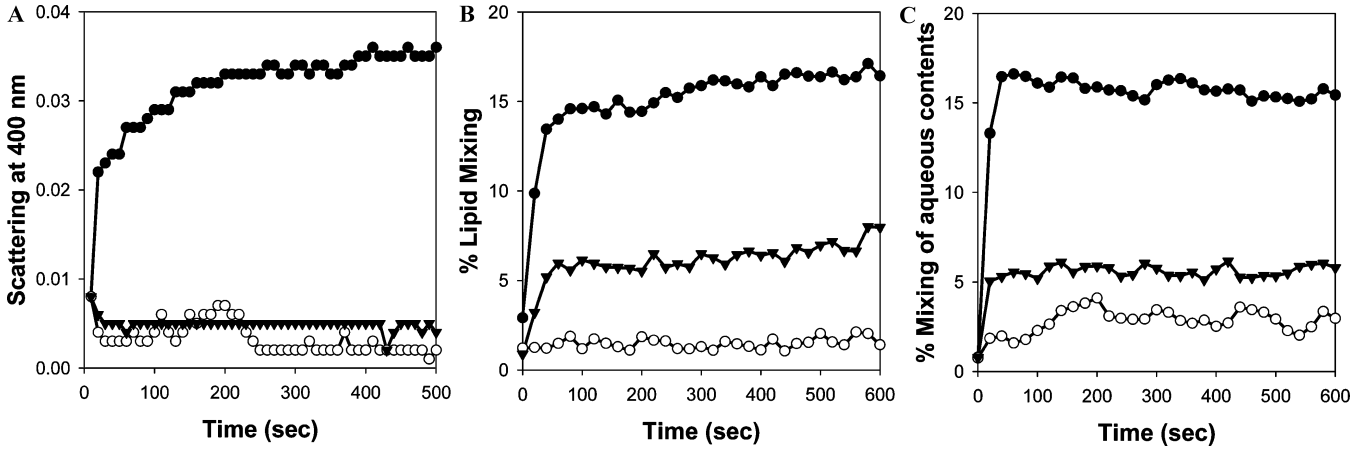

FIGURE 7: In vitro liposome aggregation and/or fusion induced by full-length BMFP and its truncated variants. (A) Time course of DPPC/DPPA SUV aggregation monitored by light scattering. (B) Time course of lipid mixing (DPPC/DPPA LUV and DPPC/DPPA LUV containing 0.6 mol % NBD-PE and Rho-PE were used in a 4:1 ratio). (C) Time course of aqueous content mixing. Equimolar amounts of terbium (Tb)- and dipicolinic acid (DPA)-loaded SUV were premixed in 10 mM Tris-HCl (pH 8.0), 50 mM NaCl, and 1 mM EDTA. The fluorescence of the $Tb(DPA)_3$ complex formed after the mixing of aqueous contents by protein addition was measured at 545 nm over incubation time. All the measurements were taken in 50 mM Tris-HCl buffer (pH 8.0) at 25 °C. The liposomes were composed of DPPC and DPPA in a molar ratio of 75:25. The lipid:protein molar ratio was 100: BMFP (●), BMFP-N (▼), and BMFP-C (○).

Table 3: Change in Vesicle Size Produced by the Addition of BMFP and Its Truncated Variants

	diameter[a] (nm)
DPPC/DPPA	83
DPPC/DPPA with BMFP	1826
DPPC/DPPA with BMFP-N	97
DPPC/DPPA with BMFP-C	92

[a] Vesicle size was evaluated by DLS. Measurements were taken in 50 mM Tris-HCl (pH 8.0). The SUV concentration was 250 μM, and the protein concentration was 1 μM.

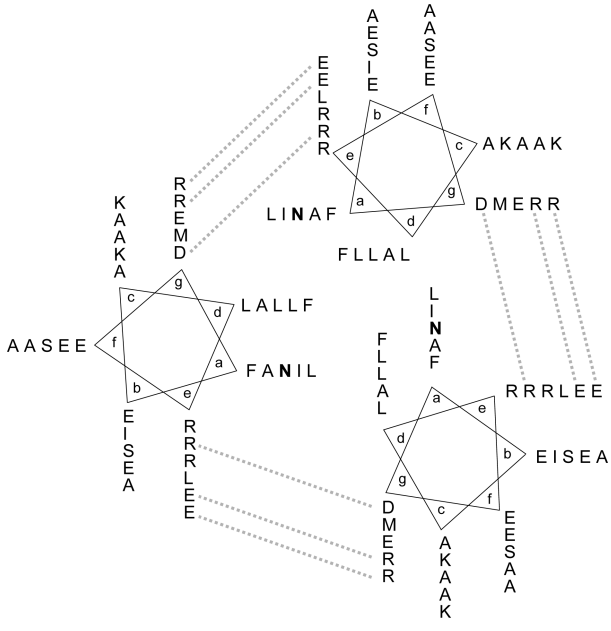

FIGURE 8: Theoretical helical wheel model of the carboxyl-terminal coiled-coil domain of BMFP.

domain, possibly by interaction through its carboxyl-terminal tail which is rich in positively charged residues.

The time courses of lipid and aqueous content mixing observed for BMFP and BMFP-N were rapid and occurred on a similar time scale. These results suggest that the process involved fast progression from "hemifusion" (when lipid leaflets mix) to complete fusion (when contents mix). Moreover, the fusion time and aggregation time observed were similar which suggest that these processes occur in parallel. In general, vesicle fusion was not induced or was less efficient with addition of the isolated BMFP domains, indicating that the full-length protein is essential for a fully in vitro fusion activity.

DISCUSSION

In this work, we present the first biophysical and biochemical characterization of BMFP. This constitutes the first step toward defining the structural and functional properties of this protein that belongs to a group of numerous protein homologues uncharacterized to date.

We showed that BMFP has two structural domains: (i) a coiled-coil C-terminal domain by which the protein self-associates as a trimer and (ii) an N-terminal domain which is disordered at neutral pH and has a propensity to adopt an amphipathic α-helical structure in the presence of phospholipid vesicles, high ionic strength, acidic pH, or SDS.

The predicted C-terminal coiled-coil region and the amphipathic α-helix of the N-terminal domain of BMFP are features highly conserved across the COG2960 proteins. These observations indicate the importance of these conserved motifs for the structure and biological function of BMFP and suggest that the properties described here for BMFP are likely to be relevant to other members of the same group. In this regard, it has to be noted that results recently obtained on BMFP homologues from *E. coli* strain K12 and *S. typhimurium* strain LT2 indicate that these proteins also are organized as trimeric structures (data not shown).

The essential feature of coiled-coil sequences is a seven-residue repeat, $(abcdefg)_n$, with the first (*a*) and fourth (*d*) positions generally occupied by hydrophobic amino acids. The other amino acids in the repeat are mostly polar. Parallel dimers and trimers are by far the most commonly observed coiled coils. In parallel coiled coils, the core (*a* and *d*) residues, which associate in register to form alternating layers, largely determine the oligomerization state. Residues at positions *e* and *g* on the edge of the helix interface also play a role in oligomer specificity (*27*).

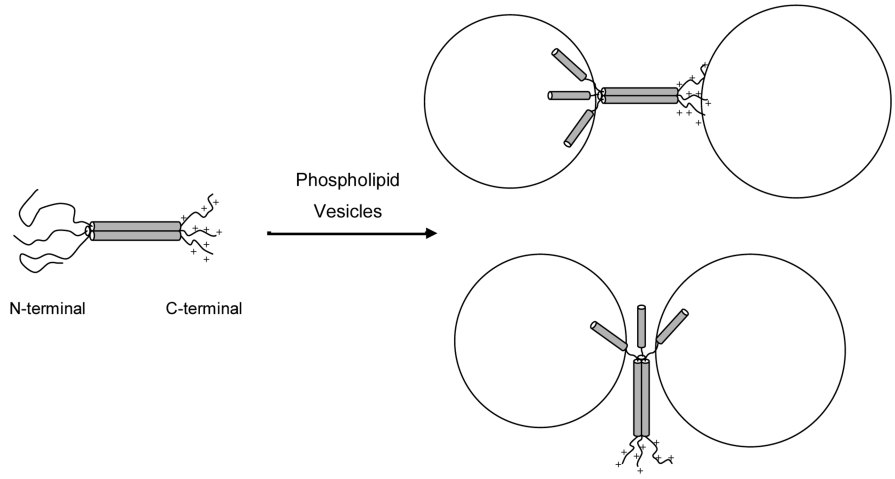

FIGURE 9: Structural model of BMFP and putative conformational changes occurring upon interaction with phospholipid vesicles.

Analysis of the sequence of the C-terminal domain of BMFP with Multicoil (http://groups.csail.mit.edu/cb/multicoil/cgi-bin/multicoil.cgi) (*28*) predicted a higher score for a two-stranded (probability, 0.6) than for a three-stranded coiled coil (probability, 0.2), in disagreement with the trimeric structure experimentally determined. As for BMFP, many short trimeric coiled-coil structures that are predicted to be dimeric exist. However, analysis of the sequence of these proteins indicated the existence of a conserved trimerization motif (R-h-x-x-h-E) that is also present in BMFP (R73−E78 and R80−E85) (*29*).

At present, we have no experimental data to postulate the parallel or antiparallel configuration of the three-stranded coiled coil of BMFP. However, N67 in position *a* would favor a parallel orientation because buried Asn residues could form an interhelical H-bond in this configuration (*30, 31*). On the basis of this assumption, we built a theoretical model of the carboxyl-terminal three-stranded coiled coil (Figure 8) in which three g−e′$_{+1}$ salt bridges between D52 and R57, R73 and E78, and R80 and E85 of contiguous chains would stabilize the coiled-coil structure. On the other hand, it has been suggested that anion binding would be a common feature of trimeric coiled coils with buried polar residues (*32*). As BMFP has N67 in position *a*, it would be interesting to investigate if this feature is related to the stabilizing effect of phosphate on the structure of the carboxyl-terminal coiled-coil domain of BMFP experimentally observed.

Our results indicate that BMFP interacts with phospholipid vesicles through a predicted amphipathic α-helix that is induced in the N-terminal half of the protein and promotes the aggregation and fusion of vesicles in vitro.

In this regard, it has to be noted that amphipathic α-helical motifs are commonly observed in natural and synthetic peptides that interact with membranes. Examples of these are pore-forming toxins such as colicin and actinoporins (*33, 34*), antimicrobial peptides such as melittin and magainin (*35*), and synthetic peptides such as GALA and Wae11 (*36, 37*). Many cytolytic and antimicrobial α-helical peptides such as melittin, magainin, alamethicin, and cecropin A exist as disordered structures in aqueous solution and fold into an α-helical conformation upon interaction with lipid surfaces. These peptides are often found to be amphipathic and can either adsorb onto membrane surface or insert into the membrane (*38*).

In the case of BMFP, although the isolated BMFP-N domain can induce vesicle fusion to some extent, the full-length protein is necessary for an efficient fusion activity.

Recent results obtained in our laboratory indicate that BMFP is an important virulence factor of *B. abortus* (S. L. Cravero et al., unpublished observations). In this regard, *Brucella* virulence mostly resides in its ability to enter, survive in, and replicate within the host cell. The survival of the bacteria in the infected cells relies upon prevention of fusion of its membrane-bound compartment, the *Brucella*-containing vacuole, with lysosomes and late endocytic vesicles (*5–7*). Whether the in vitro fusogenic activity of BMFP is related to its biological activity is uncertain and merits further investigation. However, the resemblance of BMFP structure to fusogenic proteins frequently observed in viruses, bacteria, and eukaryotes argues in favor of the biological relevance of our findings (*24, 39, 40*). The three-stranded coiled coil is a common motif found in many diverse viral membrane fusion proteins. The structures of the membrane fusion proteins of influenza virus (hemagglutinin HA2) (*41*), Moloney murine leukemia virus (MoMLV TM) (*42*), human and simian immunodeficiency viruses (HIV-1 and SIV gp41, respectively) (*43, 44*), and Ebola virus (Ebola GP2) (*45*) reveal significant similarity in their putative fusogenic (i.e., fusion-active) conformations. All five proteins contain a parallel homotrimeric coiled coil adjacent to the fusion peptide regions.

In spite of the structural similarity of these proteins to BMFP, there are also significant differences and the fusion mechanism of BMFP could be different from the virus mechanism. In viral membrane fusion proteins, there are two membrane interaction domains: (i) a C-terminal membrane anchor in the viral envelope and (ii) an N-terminal hydrophobic fusion peptide that, when exposed, interacts with the target cell membrane (*46*). In BMFP, a membrane interaction domain could be the amphipathic N-terminal α-helix, but there is no other membrane interaction domain of the type observed in the viral proteins. However, a region rich in positively charged residues located near the C-terminal end of the protein could possibly interact with membranes (Figure 9). Some evidence of this hypothesis is the fact that the isolated C-terminal domain does not fuse but induces aggregation of phospholipid vesicles in addition to a reduced

sensitivity to protease cleavage of the C-terminal tail observed in the presence of phospholipid vesicles (data not shown).

It is also possible that the in vitro fusogenic activity of BMFP would not be related to the in vivo function of this protein. Indeed, fusion of artificial membranes can be induced by numerous amphiphilic agents, including peptides and certain proteins that are clearly not involved in biological fusion reactions (*47*).

Uncovering the function of a protein is not a simple task. Sequence and structural similarity can give some clues about the natural function. However, proteins like BMFP with no determined structure and no clear sequence homology to any protein of known function are certainly very difficult to study. In these cases, subtle sequence or structural similarities to other proteins may be taken into consideration and the putative functions tested at the cellular level. In this regard, sequence comparison of BMFP with the p-FAM database (http://www.sanger.ac.uk/Software/Pfam/) (*17*) indicates that the N-terminal domain of the protein has a low similarity score with respect to SNARE proteins (Q-SNARE). Curiously, eukaryotic vesicle and target membrane SNARE proteins contribute helices to form a tetrameric coiled-coil complex which is essential for membrane fusion underlying intracellular trafficking and exocytosis (*17*). The complex includes three Q-SNARE proteins and one R-SNARE protein. Thus, it is intriguing whether BMFP could, by homology with Q-SNARE, promiscuously interact with a R-SNARE protein and perturb the normal intracellular trafficking and fusion of vesicles in the animal host. Several examples of SNARE proteins inhibited by an excess of soluble SNARE motifs acting as competitive inhibitors have been described previously (*48, 49*). Other hypothetical functions could also be evaluated. A bioinformatic analysis based on a genomic context approach (*50, 51*) predicts that the COG2960 family members would be related to protein biosynthesis. This approach predicts functional associations between protein-coding genes by analyzing gene fusion events, the conservation of gene neighborhood, or the significant co-occurrence of genes across different species. In this regard, it would be interesting to test whether BMFP could have some chaperone activity by binding to hydrophobic surfaces exposed on misfolded proteins. It would also be interesting to see if BMFPs share some common functional property with the heat shock transcription factor binding protein which is also a small trimeric coiled-coil protein very similar in general terms to BMFP (*52*).

In summary, in this work we describe a preliminary model of the structure of BMFP, the conformational changes produced under different experimental conditions, and an in vitro membrane fusogenic activity. Additional studies are required to clarify the role of BMFP in vivo, but it is expected that the structural and biochemical features of this protein described herein will be particularly important for further investigations.

ACKNOWLEDGMENT

Our thanks to Dr. Prat Gay and his laboratory for their assistance with the CD spectroscopy measurements and to Dr. Ana Cauerhff for her help with the dynamic light scattering measurements.

SUPPORTING INFORMATION AVAILABLE

Additional figures showing limited proteolysis experiments, CD spectra of BMFP and truncated variants under different conditions (ionic strength, pH, and SDS), and interaction of BMFP with lipid vesicles as a function of vesicle composition and concentration. This material is available free of charge via the Internet at http://pubs.acs.org.

REFERENCES

1. Corbel, M. J. (1997) Brucellosis: An overview. *Emerging Infect. Dis. 3*, 213–221.
2. DelVecchio, V. G., Kapatral, V., Redkar, R. J., Patra, G., Mujer, C., Los, T., Ivanova, N., Anderson, I., Bhattacharyya, A., Lykidis, A., Reznik, G., Jablonski, L., Larsen, N., D'Souza, M., Bernal, A., Mazur, M., Goltsman, E., Selkov, E., Elzer, P. H., Hagius, S., O'Callaghan, D., Letesson, J. J., Haselkorn, R., Kyrpides, N., and Overbeek, R. (2002) The genome sequence of the facultative intracellular pathogen *Brucella melitensis*. *Proc. Natl. Acad. Sci. U.S.A. 99*, 443–448.
3. Jones, S. M., and Winter, A. J. (1992) Survival of virulent and attenuated strains of *Brucella abortus* in normal and gamma interferon-activated murine peritoneal macrophages. *Infect. Immun. 60*, 3011–3014.
4. Detilleux, P. G., Deyoe, B. L., and Cheville, N. F. (1990) Penetration and intracellular growth of *Brucella abortus* in non-phagocytic cells in vitro. *Infect. Immun. 58*, 2320–2328.
5. Gorvel, J. P., and Moreno, E. (2002) *Brucella* intracellular life: From invasion to intracellular replication. *Vet. Microbiol. 90*, 281–297.
6. Roop, R. M., II, Bellaire, B. H., Valderas, M. W., and Cardelli, J. A. (2004) Adaptation of the Brucellae to their intracellular niche. *Mol. Microbiol. 52*, 621–630.
7. Porte, F., Liautard, J. P., and Kohler, S. (1999) Early acidification of phagosomes containing *Brucella suis* is essential for intracellular survival in murine macrophages. *Infect. Immun. 67*, 4041–4047.
8. Lopez-Goni, I., Guzman-Verri, C., Manterola, L., Sola-Landa, A., Moriyon, I., and Moreno, E. (2002) Regulation of *Brucella* virulence by the two-component system BvrR/BvrS. *Vet. Microbiol. 90*, 329–339.
9. Boschiroli, M. L., Ouahrani-Bettache, S., Foulongne, V., Michaux-Charachon, S., Bourg, G., Allardet-Servent, A., Cazevieille, C., Lavigne, J. P., Liautard, J. P., Ramuz, M., and O'Callaghan, D. (2002) Type IV secretion and *Brucella* virulence. *Vet. Microbiol. 90*, 341–348.
10. Roop, R. M., II, Gee, J. M., Robertson, G. T., Richardson, J. M., Ng, W. L., and Winkler, M. E. (2003) *Brucella* stationary-phase gene expression and virulence. *Annu. Rev. Microbiol. 57*, 57–76.
11. Lapaque, N., Moriyon, I., Moreno, E., and Gorvel, J. P. (2005) *Brucella* lipopolysaccharide acts as a virulence factor. *Curr. Opin. Microbiol. 8*, 60–66.
12. Berman, H. M., Westbrook, J., Feng, Z., Gilliland, G., Bhat, T. N., Weissig, H., Shindyalov, I. N., and Bourne, P. E. (2000) The Protein Data Bank. *Nucleic Acids Res. 28*, 235–242.
13. Karimova, G., Pidoux, J., Ullmann, A., and Ladant, D. (1998) A bacterial two-hybrid system based on a reconstituted signal transduction pathway. *Proc. Natl. Acad. Sci. U.S.A. 95*, 5752–5756.
14. Andrade, M. A., Chacon, P., Merelo, J. J., and Moran, F. (1993) Evaluation of secondary structure of proteins from UV circular dichroism spectra using an unsupervised learning neural network. *Protein Eng. 6*, 383–390.
15. Pecheur, E. I., Hoekstra, D., Sainte-Marie, J., Maurin, L., Bienvenue, A., and Philippot, J. R. (1997) Membrane anchorage brings about fusogenic properties in a short synthetic peptide. *Biochemistry 36*, 3773–3781.
16. Duzgunes, N., and Wilschut, J. (1993) Fusion assays monitoring intermixing of aqueous contents. *Methods Enzymol. 220*, 3–14.
17. Finn, R. D., Mistry, J., Schuster-Bockler, B., Griffiths-Jones, S., Hollich, V., Lassmann, T., Moxon, S., Marshall, M., Khanna, A., Durbin, R., Eddy, S. R., Sonnhammer, E. L., and Bateman, A. (2006) Pfam: Clans, web tools and services. *Nucleic Acids Res. 34*, D247–D251.
18. Rost, B., Yachdav, G., and Liu, J. (2004) The PredictProtein server. *Nucleic Acids Res. 32*, W321–W326.

19. Berger, B., Wilson, D. B., Wolf, E., Tonchev, T., Milla, M., and Kim, P. S. (1995) Predicting coiled coils by use of pairwise residue correlations. *Proc. Natl. Acad. Sci. U.S.A. 92*, 8259–8263.
20. Mitra, N., Sinha, S., Kini, R. M., and Surolia, A. (2005) Analysis of the peanut agglutinin molten globule-like intermediate by limited proteolysis. *Biochim. Biophys. Acta 1725*, 283–289.
21. Kalaycioglu, S., Imren, Y., Erer, D., Zor, H., and Arman, D. (2005) *Brucella* endocarditis with repeated mitral valve replacement. *J. Cardiovasc. Surg. 20*, 189–192.
22. Romero, P., Obradovic, Z., and Dunker, A. K. (1997) Sequence Data Analysis for Long Disordered Regions Prediction in the Calcineurin Family. *Genome Inf. 8*, 110–124.
23. Uversky, V. N. (2002) What does it mean to be natively unfolded? *Eur. J. Biochem. 269*, 2–12.
24. Dutch, R. E., Jardetzky, T. S., and Lamb, R. A. (2000) Virus membrane fusion proteins: Biological machines that undergo a metamorphosis. *Biosci. Rep. 20*, 597–612.
25. Huang, Q., Sivaramakrishna, R. P., Ludwig, K., Korte, T., Bottcher, C., and Herrmann, A. (2003) Early steps of the conformational change of influenza virus hemagglutinin to a fusion active state: Stability and energetics of the hemagglutinin. *Biochim. Biophys. Acta 1614*, 3–13.
26. Trivedi, V. D., Yu, C., Veeramuthu, B., Francis, S., and Chang, D. K. (2000) Fusion induced aggregation of model vesicles studied by dynamic and static light scattering. *Chem. Phys. Lipids 107*, 99–106.
27. Lupas, A. (1996) Coiled coils: New structures and new functions. *Trends Biochem. Sci. 21*, 375–382.
28. Wolf, E., Kim, P. S., and Berger, B. (1997) MultiCoil: A program for predicting two- and three-stranded coiled coils. *Protein Sci. 6*, 1179–1189.
29. Kammerer, R. A., Kostrewa, D., Progias, P., Honnappa, S., Avila, D., Lustig, A., Winkler, F. K., Pieters, J., and Steinmetz, M. O. (2005) A conserved trimerization motif controls the topology of short coiled coils. *Proc. Natl. Acad. Sci. U.S.A. 102*, 13891–13896.
30. Woolfson, D. N., and Alber, T. (1995) Predicting oligomerization states of coiled coils. *Protein Sci. 4*, 1596–1607.
31. Gonzalez, L., Jr., Woolfson, D. N., and Alber, T. (1996) Buried polar residues and structural specificity in the GCN4 leucine zipper. *Nat. Struct. Biol. 3*, 1011–1018.
32. Eckert, D. M., Malashkevich, V. N., and Kim, P. S. (1998) Crystal structure of GCN4-pIQI, a trimeric coiled coil with buried polar residues. *J. Mol. Biol. 284*, 859–865.
33. White, D., Musse, A. A., Wang, J., London, E., and Merrill, A. R. (2006) Toward elucidating the membrane topology of helix two of the colicin E1 channel domain. *J. Biol. Chem. 281*, 32375–32384.
34. Malovrh, P., Viero, G., Serra, M. D., Podlesek, Z., Lakey, J. H., Macek, P., Menestrina, G., and Anderluh, G. (2003) A novel mechanism of pore formation: Membrane penetration by the N-terminal amphipathic region of equinatoxin. *J. Biol. Chem. 278*, 22678–22685.
35. Bechinger, B. (1999) The structure, dynamics and orientation of antimicrobial peptides in membranes by multidimensional solid-state NMR spectroscopy. *Biochim. Biophys. Acta 1462*, 157–183.
36. Pecheur, E. I., Martin, I., Ruysschaert, J. M., Bienvenue, A., and Hoekstra, D. (1998) Membrane fusion induced by 11-mer anionic and cationic peptides: A structure-function study. *Biochemistry 37*, 2361–2371.
37. Parente, R. A., Nir, S., and Szoka, F. C., Jr. (1988) pH-dependent fusion of phosphatidylcholine small vesicles. Induction by a synthetic amphipathic peptide. *J. Biol. Chem. 263*, 4724–4730.
38. Blondelle, S. E., Lohner, K., and Aguilar, M. (1999) Lipid-induced conformation and lipid-binding properties of cytolytic and antimicrobial peptides: Determination and biological specificity. *Biochim. Biophys. Acta 1462*, 89–108.
39. Hayward, R. D., McGhie, E. J., and Koronakis, V. (2000) Membrane fusion activity of purified SipB, a *Salmonella* surface protein essential for mammalian cell invasion. *Mol. Microbiol. 37*, 727–739.
40. Fasshauer, D. (2003) Structural insights into the SNARE mechanism. *Biochim. Biophys. Acta 1641*, 87–97.
41. Wilson, I. A., Skehel, J. J., and Wiley, D. C. (1981) Structure of the haemagglutinin membrane glycoprotein of influenza virus at 3 Å resolution. *Nature 289*, 366–373.
42. Fass, D., Harrison, S. C., and Kim, P. S. (1996) Retrovirus envelope domain at 1.7 angstrom resolution. *Nat. Struct. Biol. 3*, 465–469.
43. Chan, D. C., Fass, D., Berger, J. M., and Kim, P. S. (1997) Core structure of gp41 from the HIV envelope glycoprotein. *Cell 89*, 263–273.
44. Malashkevich, V. N., Chan, D. C., Chutkowski, C. T., and Kim, P. S. (1998) Crystal structure of the simian immunodeficiency virus (SIV) gp41 core: Conserved helical interactions underlie the broad inhibitory activity of gp41 peptides. *Proc. Natl. Acad. Sci. U.S.A. 95*, 9134–9139.
45. Malashkevich, V. N., Schneider, B. J., McNally, M. L., Milhollen, M. A., Pang, J. X., and Kim, P. S. (1999) Core structure of the envelope glycoprotein GP2 from Ebola virus at 1.9-Å resolution. *Proc. Natl. Acad. Sci. U.S.A. 96*, 2662–2667.
46. Gallaher, W. R. (1987) Detection of a fusion peptide sequence in the transmembrane protein of human immunodeficiency virus. *Cell 50*, 327–328.
47. Jahn, R., and Grubmuller, H. (2002) Membrane fusion. *Curr. Opin. Cell Biol. 14*, 488–495.
48. Scales, S. J., Hesser, B. A., Masuda, E. S., and Scheller, R. H. (2002) Amisyn, a novel syntaxin-binding protein that may regulate SNARE complex assembly. *J. Biol. Chem. 277*, 28271–28279.
49. Hatsuzawa, K., Lang, T., Fasshauer, D., Bruns, D., and Jahn, R. (2003) The R-SNARE motif of tomosyn forms SNARE core complexes with syntaxin 1 and SNAP-25 and down-regulates exocytosis. *J. Biol. Chem. 278*, 31159–31166.
50. Doerks, T., von Mering, C., and Bork, P. (2004) Functional clues for hypothetical proteins based on genomic context analysis in prokaryotes. *Nucleic Acids Res. 32*, 6321–6326.
51. Gaudermann, P., Vogl, I., Zientz, E., Silva, F. J., Moya, A., Gross, R., and Dandekar, T. (2006) Analysis of and function predictions for previously conserved hypothetical or putative proteins in *Blochmannia floridanus*. *BMC Microbiol. 6*, 1.
52. Tai, L. J., McFall, S. M., Huang, K., Demeler, B., Fox, S. G., Brubaker, K., Radhakrishnan, I., and Morimoto, R. I. (2002) Structure-function analysis of the heat shock factor-binding protein reveals a protein composed solely of a highly conserved and dynamic coiled-coil trimerization domain. *J. Biol. Chem. 277*, 735–745.

BI800462Y